International Journal of Heat and Mass Transfer 52 (2009) 1657–1666

Contents lists available at ScienceDirect

International Journal of Heat and Mass Transfer

journal homepage: www.elsevier.com/locate/ijhmt

Numerical modeling of axial bed-to-wall heat transfer in a circulating fluidized bed combustor

Nirmal V. Gnanapragasam [a], Bale V. Reddy [b,*]

[a] Department of Mechanical Engineering, University of New Brunswick, Fredericton, NB, Canada E3B 5A3
[b] Faculty of Engineering and Applied Sciences, University of Ontario Institute of Technology, Oshawa, Ont., Canada L1H 7K4

ARTICLE INFO

Article history:
Received 2 February 2008
Received in revised form 8 October 2008
Available online 6 December 2008

Keywords:
Circulating fluidized bed combustor
Axial heat transfer
Gas–solid energy balance
Bed-to-wall heat transfer
Axial voidage

ABSTRACT

The water-wall surfaces located above the secondary air inlet within the circulating fluidized bed (CFB) combustor are exposed to the axial bed-to-wall heat transfer process. In the current work, the axial bed-to-wall heat transfer coefficients are estimated for three different axial voidage profiles (covering three widely occurring average particle concentrations) in order to investigate the effect of voidage, time, initial and fixed temperature of the bed and annulus, and gas gap between wall and solid particles; on the axial heat transfer process. A 2D thermal energy balance model is developed to estimate the axial heat transfer values for the gas–solid suspension along the height of the riser column with horizontally changing mass distribution. The gas–solid mass distribution is fixed with time thus providing a spectrum of changes in axial bed-to-wall heat transfer profile with time. The current work provides an opportunity to understand the axial heat transfer relationship with particle concentration and instantaneous behaviour. The results from the work show that: (i) first few seconds of the suspension temperature near the wall has maximum energy thus providing a small time frame to transfer more heat to the surface (CFB wall); (ii) both axial and horizontal particle concentrations (influenced by the operating conditions) affect the axial heat transfer locally; (iii) initial temperature of the bed between average and maximum values provide end limits for the axial heat transfer; (iv) annulus region has higher thermal energy than the core due to increased particle presence; and (v) a particle-free zone near the wall (gas gap) having a maximum thickness of 1 mm, tends to reduce up to 25% of axial heat transfer value. The model trends have close agreement with experimental trends from published literature; but the model values differ when correlating with real values due to inconsistencies in riser diameter and nature of variation in parameters.

1. Introduction

The circulating fluidized bed (CFB) combustors use coal and other solid fuels such as biomass, agricultural and municipal waste as the primary source for power generation applications. The basic principle of operation in a CFB combustor involves the suspension of solid particles by fluidizing gas facilitating better combustion and low emissions through improved heat transfer and solids handling. The axial heat transfer process within the CFB combustor occurs from the gas–solid suspension to water-wall surfaces, located along the furnace height above the secondary air inlet, providing much of the thermal energy needed for water to steam conversion. The axial heat transfer process is subject to varying conditions (hydrodynamic and thermal) due to changes in the behaviour of the gas–solid suspension mostly near the wall (annulus region). The near wall condition is the end result of changes in the core region induced by the operating conditions such as superficial gas velocity, solids circulation rate and bed temperature. Fundamental understanding of the axial heat transfer process is required for better design of heat transferring surfaces along the height of the CFB combustor. In this regard, some experimental findings are reported on the axial heat transfer profiles [1–5] but have limited analysis with respect to the effects of operating parameters on the axial heat transfer process. Reddy and Nag [6] reported axial and radial heat transfer coefficients based on experiments and empirical correlations using the dimensional analysis; they have compared the results with experimental data providing some background information on the axial heat transfer behaviour. Very few axial heat transfer models have been attempted for providing new and additional information on the axial heat transfer process occurring within the CFB combustor. The estimation of axial heat transfer coefficient by He et al. [4] based on the two-fluid model considering the fluid dynamic and continuum principles investigates the axial distribution of component heat transfers and their contributions to the total heat transfer coefficient. The effect of physical properties of solid particle (diameter, specific heat and density), gas velocity, bed and wall temperatures were analysed for the axial

* Corresponding author. Tel.: +1 905 721 3111x3661; fax: +1 905 721 3370.
E-mail addresses: Bale.Reddy@uoit.ca, bv_reddy@hotmail.com (B.V. Reddy).

0017-9310/$ - see front matter © 2008 Elsevier Ltd. All rights reserved.
doi:10.1016/j.ijheatmasstransfer.2008.10.003

Nomenclature

a	coefficient of the grid nodes in the current time step
a_P^0	coefficient of the grid node in the previous time step
a_{SSg}	coefficient for gas phase in finite volume formulation
a_{SSp}	coefficient for particle phase in finite volume formulation
A	surface area, m^2
c_p	specific heat, J/kg K
d	diameter of solid particle, mm
dx	displacement in the horizontal direction (x-direction), m
dy	displacement in the vertical direction (y-direction), m
D	diameter of riser column, m
e	emissivity
G_s	net solids circulation rate, kg/m^2 s
h	bed-to-wall heat transfer coefficient, W/m^2 K
H^-	height of the riser column, m
H_d	height of the dense bottom bed, m
H_{ex}	height of the exit region, m
H_l	height of the lean bed above dense bed, m
h_c	cluster heat transfer coefficient, W/m^2 K
h_d	dispersed (gas) phase convection heat transfer coefficient, W/m^2 K
h_p	particle heat transfer coefficient, W/m^2 K
h_{pg}	particle to gas heat transfer coefficient, W/m^2 K
h_r	radiation heat transfer coefficient, W/m^2 K
R_{fp}	radiation view factor for the particle phase
R_{fg}	radiation view factor for the gas phase
S	source term
T	temperature, K
u_g	local gas velocity, m/s
U_g	superficial net gas velocity, m/s
u_p	local particle velocity, m/s
V_p	net particle velocity, m/s

Symbols

α	volume fraction of solids
$\bar{\varepsilon}$	cross-sectional average voidage at a given axial location
εmf	minimum fluidization voidage
μ	dynamic viscosity of the gas, N s/m^2
ρ	density, kg/m^3

Subscripts

avg	average
b	bed
g	gas
j	number from 1 up to $dy * j = H$
N, E, W, S	neighbouring grid nodes in each direction
P	particle
P	grid node being estimated
r	radial or radiation heat transfer
w	wall

heat transfer process. Xie et al. [7,8] proposed a model that provides axial heat transfer profile based on the solids concentration and suspension density. This model includes particle and gas heat transfer estimation based on the assumption of parallel surfaces in the annulus region. The heat transfer profile along the height with distance from the wall; particle and gas temperature distributions and radiation flux information are also provided. Hua et al. [3] have developed a three-dimensional axial radiation heat transfer model to study the particle composition influence. In line with the model, analysis and information reported in both Xie et al. [7,8] and He et al. [4] further investigation is sought for providing instantaneous behaviour of the axial heat transfer mechanism within the CFB combustor. Especially, analyses involving the effect of time from initial to steady state for three different fixed hydrodynamic bed conditions on axial heat transfer. The time based change affecting only the heat transfer characteristics of the gas–solid suspension is essential for surface designers to understand how the CFB axial heat transfer behaves instantaneously.

The 2D numerical model of the axial heat transfer process developed for the current work is based on the gas–solid thermal energy balance with horizontally changing solids distribution all along the height of the CFB riser column. The following analyses are reported and discussed:ussed:

- *Effect of axial voidage distribution:* Test the sensitiveness of the heat transfer for three different axial particle concentration profiles. Time variation in axial heat transfer profile for each of these three solids distribution is discussed.
- *Effect of horizontal voidage distribution:* Behaviour of axial heat transfer is profiled when the horizontal particle concentration is varied. Difference in behaviour with time is also discussed.
- *Effect of bed initial temperature:* Three different bed initial temperatures (i) fixed average, (ii) fixed maximum and (iii) axially varying linear temperature profile are considered to predict the axial heat transfer profile.
- *Annulus-to-wall heat transfer:* The annulus region has the most number of solid particles across given cross-section. The heat transfer from just the annulus-to-wall is estimated to find the difference in bed and annulus thermal potential.
- *Effect of gas gap between the wall and gas–solid suspension near the wall:* A small gas gap of fixed thickness (0.1% of the riser diameter) is considered to study its resistance towards heat transfer along the height.
- The radiation from gases inside the riser column is considered for the total bed-to-wall heat transfer estimation.

The change in heat transfer with time for a given solids distribution as part of the analysis, provides essential information on temperature gradients near the wall and the influence of bed and annulus region initial temperatures. When discussing the heat transfer values with time; some of the results are displayed for different times from start and up to the steady state; and in some other results, heat transfer values for only intermediate and steady state temperatures are presented.

2. Axial-horizontal mass distribution model

The typical axial flow structure comprising the major portion of the riser column of a CFB combustor is the core–annulus flow structure. Based on the solids concentration, the 'core' is defined as a relatively dilute up-flowing region in which solid particles are entrained upward by the high-velocity gas stream such that the gas with few particles, flow upwards in the centre of the riser column. The 'annulus' is a much denser and smaller region near the wall in which solid particles congregate and fall down as dense structures similar to wave of strands or streamers termed as the "clusters". Several cluster based numerical heat transfer works have been published [9–12] with characterization of the cluster parameters and operating conditions on local heat transfer. In this work, the cluster hydrodynamics is represented by the axial voidage profiles of Monazam et al. [2] which are used as input to

the local mass distribution which is estimated for every location along the height.

The mass flux balance model of He et al. [4] estimates the core–annulus voidage based on fixed horizontal voidage within the annulus and the core. The horizontal voidage distribution within the annulus and some portions of the core is used for each axial location to estimate the solids concentration distribution for the 2D grid, without a mass flux balance. The He et al. [4] mass flux balance model is not good for *small laboratory-scale* CFB units having smaller diameters ($D \leqslant 1$ m) due to the limitation in parameter estimation within the model. Similar restrictions (riser diameter should be $D \geqslant 0.5$ m) apply to the current voidage model as well for the correlation in Eq. (1). The 2D model domain for the CFB riser is shown in Fig. 1; the current model provides heat transfer prediction only for the region above H_d for core–annulus voidage solution and the region spanning entire H for horizontal voidage solution. The voidage information is estimated for each cross-section averaged voidage along the height of the riser column based on variable horizontal voidage correlation from Issangya et al. [13],

$$\varepsilon_r = \varepsilon_{mf} + (\bar{\varepsilon} - \varepsilon_{mf})\bar{\varepsilon}^{(-1.5+2.1(r/R)^{3.1}+5(r/R)^{8.8})} \quad (1)$$

Here ϵ_{mf} is the voidage of the bed at minimum fluidization velocity. For the current analysis it is a fixed value as given in Table 1. The average voidage $\bar{\varepsilon}$ in Eq. (1) will be provided as an input from the three different pre-defined axial voidage distributions as shown in Fig. 2. For each $\bar{\varepsilon}$ there will be a voidage value at every horizontal location on the given axial location. Having estimated the voidage along the y-direction (axial) and along the x-direction (horizontal), every node in the 2D grid has an associated property such as voidage, particle velocity and gas velocity. This information is fed to the thermal energy balance model for the gas and solid phases whose formulation and estimation is discussed in the next section towards the estimation of axial heat transfer coefficients.

3. Energy balance model formulation

The thermal energy balance between the solid particles and gas inside the riser column is achieved based on two simultaneous

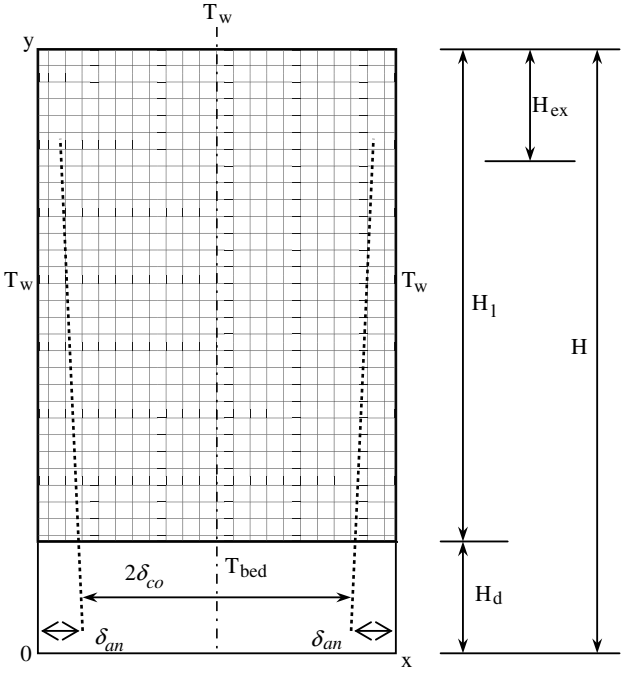

Fig. 1. The 2D model domain for the CFB riser showing core–annulus thickness along with the boundary conditions.

Table 1
Values of physical properties and parameter values used in the current model.

Solid particle (sand): He et al. [4]	$\rho_p = 2600$ kg/m^3, $k_p = 0.27$ W/mK $c_{pp} = 850$ J/kg K, $e_p = 0.85$
Gas (air):	$\rho_g = 351/T_{avg}$ kg/m^3
Flamant [23]	$k_g = 5.66 \times 10^{-5} T_{avg} + 1.1 \times 10^{-2}$ W/mK
Core region: $T_{avg} = T_b$ K	$c_{pg} = (0.99 + 1.22 \times 10^{-4} T_{avg}) \times 10^3$– $(5.68 \times 10^3 T_{avg}^{-2}) \times 10^3$ J/kg K
Annulus region: $T_{avg} = (T_b + T_w)/2$ K	$\mu_g = 0.42 \times 10^{-6} T_{avg}^{2/3}$ Ns/m^2
Parameter values:	$d_p = 250$ μm, $e_w = 0.8$, $e_g = 0.15$, $\varepsilon_{mf} = 0.45$
Operating conditions:	$T_b = 1100$ K and $T_w = 600$ K $U_g = 3.87$ m/s $G_s = 2.4, 5.6, 11.4$ kg/m^{2}s
Initial and boundary conditions:	$T_{init} = T_b$, T_{avg}, T_{linear} $T_{BC} = T_b$, T_w
2D domain grid details:	$H = 15$ m, $D = 1$ m, $X = 1000$, $Y = 1000$, $\Delta x = 0.001$, $\Delta y = 0.015$, $\Delta t = 0.001$ s

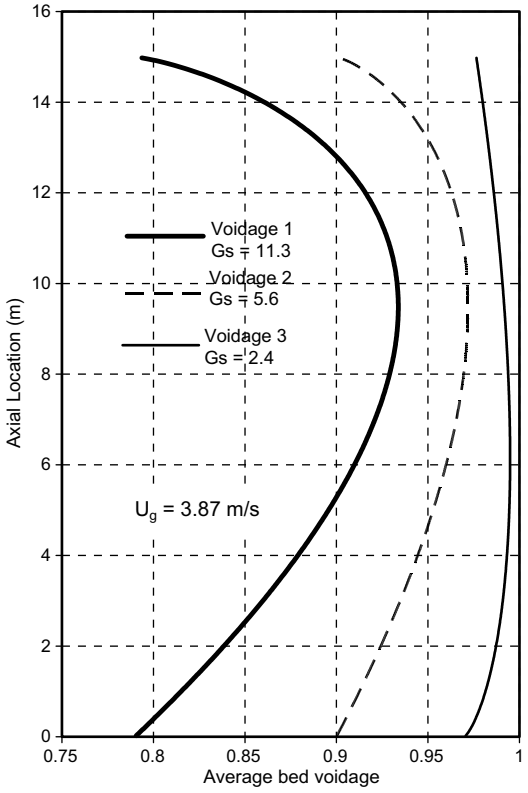

Fig. 2. Three different test axial average voidage distributions traced from Monazam et al. [2] used as input to the mass distribution model in Eq. (1).

processes. One is the balance of the rate of change internal energy of the particles or gas and the rate of heat loss for particles to gas or heat gain for gas from particles. The other is the balance between the conduction within the particle or gas nodes and the corresponding convection to the surroundings. This is summarized in Eq. (2) for gas phase and Eq. (3) for particle/solid phase. Thermal energy balance for the *gas phase* is represented by

$$\rho_g c_{pg} \alpha_g \frac{\partial T_g}{\partial t} + \rho_g c_{pg} u_g \alpha_g \frac{\partial T_g}{\partial y} = \frac{\partial}{\partial x}\left(k_g \frac{\partial T_g}{\partial x}\right) + \frac{\partial}{\partial y}\left(k_g \frac{\partial T_g}{\partial y}\right) + R_{fg} T_g^3 \left(\frac{\partial T_g}{\partial x} + \frac{\partial T_g}{\partial y}\right) + h_{pg} A (T_p - T_g) \quad (2)$$

Thermal energy balance for the *solid phase* is represented below, with a modified radiation source term, similar to the one used in the cluster energy balance model in chapter 4.

$$\rho_p c_{pp}\alpha_p\frac{\partial T_p}{\partial t}+\rho_p c_{pp}u_p\alpha_p\frac{\partial T_p}{\partial y}=\frac{\partial}{\partial x}\left(k_p\frac{\partial T_p}{\partial x}\right)+\frac{\partial}{\partial y}\left(k_p\frac{\partial T_p}{\partial y}\right)+R_{fp}T_p^3\left(\frac{\partial T_p}{\partial x}+\frac{\partial T_p}{\partial y}\right)+h_{pg}A(T_p-T_g) \quad (3)$$

Here $\alpha_g = \epsilon_r$, $\alpha = 1-\epsilon$ are volume fractions of gas and solid particles (the voidage in the core and annulus for the gas phase and particle concentration in the core and annulus for the solid phase) which are defined based on the mass flux balance. The heat transfer coefficient between the solid and gas phases h_{pg} is estimated using the Nusselt number correlation of Richardson and Ayers [14]. k_p, k_g are the thermal conductivities of the solid and gas phases. u_g, u_p are the velocities of gas and solid particles, respectively.

The radiation source terms (third term on the right hand side) in Eqs. (2) and (3) are obtained from the derivative of the Stefan–Boltzmann law (σT^4) as discussed in Gnanapragasam [15]. Since the main analysis in the current work involved is the influence of time, voidage and initial conditions on axial heat transfer, only the basic form of the radiation source term is used in the gas–solid thermal energy balance model. An advanced source term with improved accountability of radiation parameters can be found in He et al. [4] and Eriksson and Golriz [16]. The radiation source factor used in the radiation source term for the gas phase (Eq. (2)) includes the radiation view factor weighted by the voidage,

$$R_{fg}=4\sigma\left(\frac{1}{e_g}+\frac{1}{e_w}-1\right)^{-1} \quad (4)$$

The radiation source factor used in the radiation source term for the particle phase (Eq. (3)) includes the radiation view factor weighted by the solids concentration,

$$R_{fp}=4\sigma\left(\frac{1}{e_p}+\frac{1}{e_w}-1\right)^{-1} \quad (5)$$

Due to the nature of hydrodynamics of the gas–solid phase in the CFB combustor, majority of the particles reside very close to the wall (annulus region), thus the emissivity of the wall is also included in estimating the radiation source factors in Eqs. (4) and (5). Under dilute (low particle region in the core of the column above the bottom bed) conditions along the height of the column the use of wall emissivity will help in accounting the proper thermal radiation values for particle-to-wall and gas-to-wall heat transfer. Though for the core region, emissivity of particle could be used in Eq. (4) while emissivity of gas could be used in Eq. (5). But here the link between CFB wall and gas–solid suspension is enhanced by including the wall emissivity for the radiation view factor estimation within the 2D domain.

The finite volume method is used to discretize these Eqs. (2) and (3) to be applied in the 2D grid of the riser column. The finite volume method formulation is based on the details presented in Patankar [17] and Versteeg and Malalasekera [18]. The main finite volume coefficients that differ apart from others between the gas and particle phases are given here;

$$a_{SSg}=\frac{\rho_g c_{pg}u_g A_p}{\Delta y},\quad a_{SSgx}=\frac{R_{fg}A_p}{\Delta x},\quad a_{SSgy}=\frac{R_{fg}A_p}{\Delta y} \quad (6)$$

$$a_{SSp}=\frac{\rho_p c_{pp}\alpha_p u_p A_P}{\Delta y},\quad a_{SSpx}=\frac{R_{fp}A_P}{\Delta x},\quad a_{SSpy}=\frac{R_{fp}A_P}{\Delta y} \quad (7)$$

The final form of the discretized equation one for each phase becomes

$$a_P T_P = a_E T_E + a_W T_W + a_S T_S + a_N T_N + a_P^0 T_P^0 + S_C \quad (8)$$

where a's are coefficients for the respective neighbouring node temperatures in the 2D grid for the riser column and $a_P = a_P^0 + a_E + a_W + a_S + a_N - S_P$ will be the source term for the temperature of the gas or solid node currently estimated within the same time step. The particle to gas convection is estimated based on the Nusselt number correlation of Richardson and Ayers [14] as given below

$$h_{pg}=0.054\mathrm{Re}_p^{1.28}\left(\frac{k_g}{d_p}\right) \quad (9)$$

The net particle velocity in the riser column is estimated from the following relation, which is a function of the solids circulation rate,

$$V_p=\frac{G_s}{\rho_p(1-\bar{\varepsilon})} \quad (10)$$

With the help of tri-diagonal matrix algorithm (TDMA) all the nodes are solved for each time step till steady state is reached. The 2D temperature profile for gas and solid phase obtained through the solution of the model will be used for the respective heat transfer coefficient estimation. The sequence of the entire procedure is shown in Fig. 3 for the axial mass distribution model with gas–solid energy balance. The steps in the flow charts are repeated for each operating condition and analysis settings. As for the model it is assumed that the wall is covered with either particles or gas at all times; the bottom bed is not included in the analysis, though the values are provided; fixed temperatures are used for initial and boundary conditions; and the mass distribution of gas–particle in the entire riser is fixed with time. This model has its own limitations; the core-shrinking solids distribution along the height may not be the same as in the real CFB unit, since the distribution does not change with time; the momentum of the particles and its effects on heat transfer are not included in the model and the model neglects horizontal velocity components for gas and solid particles in both core and annulus regions.

4. Heat transfer estimation

4.1. Bed-to-wall heat transfer coefficients

The boundary of the control volume facing the wall starts loosing heat to the wall and a temperature profile sets inside the annulus region when it reaches steady state for the given mass flux balance. From this temperature profile, component heat transfer coefficients is estimated using the conduction–convection relation. The *particle* convective heat transfer coefficient at a given axial location near the riser wall is estimated as;

$$h_p=k_p\frac{(T_{px}-T_w)}{\Delta x(T_b-T_w)} \quad (11)$$

where 'px' is the grid node next to the wall of the riser column for the particle/solid phase. The *gas* convective heat transfer coefficient at a given axial location near the riser wall is estimated as;

$$h_g=k_g\frac{(T_{gx}-T_w)}{\Delta x(T_b-T_w)} \quad (12)$$

where 'gx' is the grid node next to the wall of the riser column for the gas phase. The *radiation* heat transfer coefficient from the particles to the wall is given below;

$$h_{rp}=R_{fp}(T_{px}+T_w)(T_{px}^2+T_w^2)/4 \quad (13)$$

The *radiation* heat transfer coefficient from the gas to the wall is given below;

$$h_{rg}=R_{fg}(T_{gx}+T_w)(T_{gx}^2+T_w^2)/4 \quad (14)$$

The overall *bed-to-wall* heat transfer coefficient is summarized as the simple addition of heat transfer from the gas–solid suspension through particle–gas convection and particle–gas radiation is;

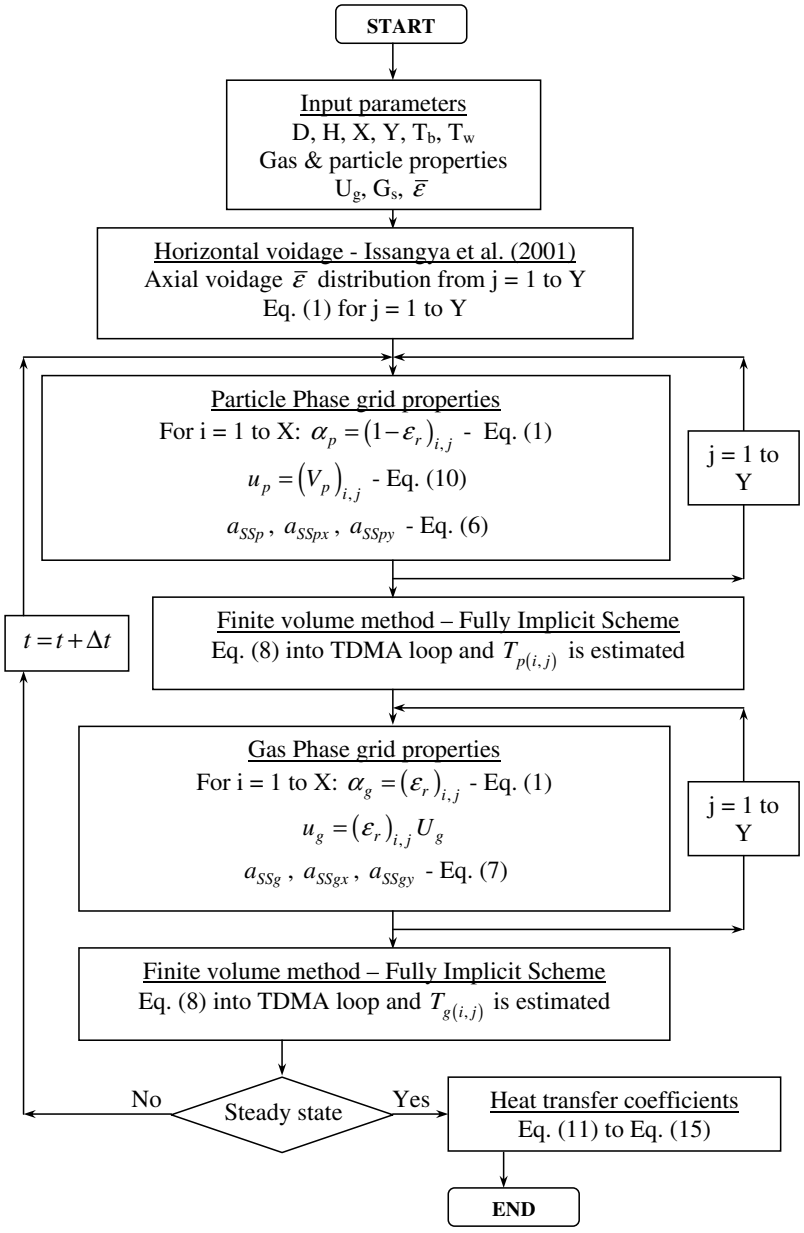

Fig. 3. Sequence of calculation procedure in estimating the axial heat transfer coefficients for the current model using Issangya et al. [13] correlation.

$$h = h_p + h_g + h_{rp} + h_{rg} \tag{15}$$

4.2. Annulus-to-wall heat transfer coefficients

The estimation of heat transfer coefficient based on the difference between the bed and the wall temperature adjacent may not be realistic for continuously changing conditions near the wall. For certain situations in the bed, having the bulk temperature difference of the bed and wall would be too high. A different representation of the heat transfer coefficient to the wall is presented here; using the average annulus temperature to estimate the component heat transfer coefficients. Thus, the *particle* convective heat transfer coefficient at a given axial location in the annulus is estimated as;

$$h_{pan} = k_p \frac{(T_p - T_w)}{\Delta x(\overline{T_{pan}} - T_w)} \tag{16}$$

where 'pan' represents the bulk temperature of the particle/solid phase in the annulus region. The *gas* convective heat transfer coefficient at a given axial location in the annulus is estimated as;

$$h_{gan} = k_g \frac{(T_g - T_w)}{\Delta x(\overline{T_{gan}} - T_w)} \tag{17}$$

where 'gan' represents the bulk temperature of the gas phase in the annulus region. The *radiation* heat transfer coefficients, from the particle to the wall and from gas to the wall are estimated same as given in Eqs. (13) and (14). The *annulus-to-wall* heat transfer coefficient is summarized as;

$$h_{an} = h_{pan} + h_{gan} + h_{rp} + h_{rg} \tag{18}$$

4.3. Axial bed temperature

The axial bed temperature is estimated for calculating heat transfer coefficients based on the temperature of particle and gas

at all nodes. Based on the horizontal voidage distribution, the temperature of the bed along the height is calculated for each location by adding and averaging the horizontal gas and particle temperatures as given below,

$$\overline{T_{Bpg}} = [(1-\varepsilon_r)T_p + \varepsilon_r T_g]/X \tag{19}$$

The temperatures of solid particles and gas have been estimated based on respective densities and specific heats. But here in Eq. (19) the temperature average is estimated based only on the volume fraction (voidage) of the gas and solid (along with the respective temperatures), so that the impact of voidage alone is realized when calculating the heat transfer coefficient, whose effect is discussed along with the results. The *particle* convective heat transfer coefficient at a given axial location based on $\overline{T_{Bpg}}$ is;

$$h_{p-TBpg} = k_p \frac{(T_p - T_w)}{\Delta x(\overline{T_{Bpg}} - T_w)} \tag{20}$$

The *gas* convective heat transfer coefficient at a given axial location based on $\overline{T_{Bpg}}$ is;

$$h_{g-TBpg} = k_g \frac{(T_g - T_w)}{\Delta x(\overline{T_{Bpg}} - T_w)} \tag{21}$$

The *radiation* heat transfer coefficients, from the particle to the wall and from gas to the wall are estimated same as given in Eqs. (13) and (14). The heat transfer coefficient based on the axial bed temperature is summarized as;

$$h_{TBpg} = h_{p-TBpg} + h_{g-TBpg} + h_{rp} + h_{rg} \tag{22}$$

The addition of heat transfer components in Eqs. (15), (18) and (22) accounts for the component heat transfer coefficients since all these components are estimated at the same time for each axial location near the wall of the riser column. The addition of the component heat transfer coefficients is also based on the assumption that the wall is continuously covered by the gas–solid suspension depending on the local voidage.

5. Results and discussion

The thermo-physical properties, range of operating parameters, initial and boundary conditions, and 2D grid parameters are given in Table 1. The gas velocity and the solids circulation rate are lower than the typical range for commercial CFB combustors. Since the model and analysis is mainly aimed at studying the influence of axial voidage profile on the heat transfer, the axial voidage profile from an experimental setup [2] is used here with the same operating conditions as shown in Fig. 2. The 2D grid for the mass distribution and heat transfer domain along with boundary conditions is shown in Fig. 1 is divided into smaller cells in both *X* and *Y* directions. The analysis includes the effect of operating parameters such as superficial gas velocity and solids circulation rate, the effect of axial and horizontal voidage, effect of initial temperatures, gas gap along with the three different heat transfer coefficient estimations described in Section 4.

5.1. Effect of axial average voidage distribution

The mass flux balance model provided by He et al. [4] gives imbalance in core–annulus voidage when used for riser diameters less than 1 m. So the Issangya et al. [13] correlation in Eq. (1) is used to estimate the horizontal voidage for every axial cross-section averaged voidage along the height. Three different axial voidage distributions are used which follow the profiles and operating conditions from the experimental data of Monazam et al. [2]. These three voidage distribution forms the input to the new 2D voidage distribution model. The voidage profiles were generated using trial and error fit of curve using logarithmic series and are shown in Fig. 2. Now based on the horizontal voidage distribution along the width and height of the riser (2D grid) column, the corresponding heat transfer coefficients are estimated using the thermal energy balance model as discussed previously and explained in sequence in Fig. 3. The voidage profiles are named 'Voidage 1', '2' and '3', respectively, with different solids circulation rates and same superficial gas velocity. The voidage profiles in the annulus will have values that are almost half of the average voidage, suggesting that the annulus has about 50% higher particles than the core region at any given location based on the average voidage at that location.

The change in axial heat transfer coefficient with time for the three voidage is shown in Figs. 4–6. The voidage 1 has higher particle concentration in bottom and top, thus the profile of heat transfer reflects the change in voidage even at steady state in the bottom region. The heat transfer coefficient value of voidage 2 does not change much with height and remains almost the same except in the bottom region. Similar to large CFB combustors, there is rapid change in heat transfer values with time for all the three cases of voidage. The difference in heat transfer between 5 and 10 s is higher for voidage 2 than voidage 1. This shows the effectiveness of higher solids concentration (in voidage 1) to hold-up the thermal energy, while the voidage 2 does not have the same thermal potential due to lower solids concentration in most of the axial location. The axial change in bed-to-wall heat transfer coefficient for the third voidage distribution is shown in Fig. 6 with time. Again there is very little change along the height. The difference in heat transfer value from 5 to 10 s shows that the riser with such a voidage distribution will be having unstable bed temperatures due to faster change in the temperature profile aided by lack of solid particles. The average voidage and the solids circulation rate have a combined effect on the heat transfer profile. In the top region, the heat transfer value for voidage 1 decreases compared

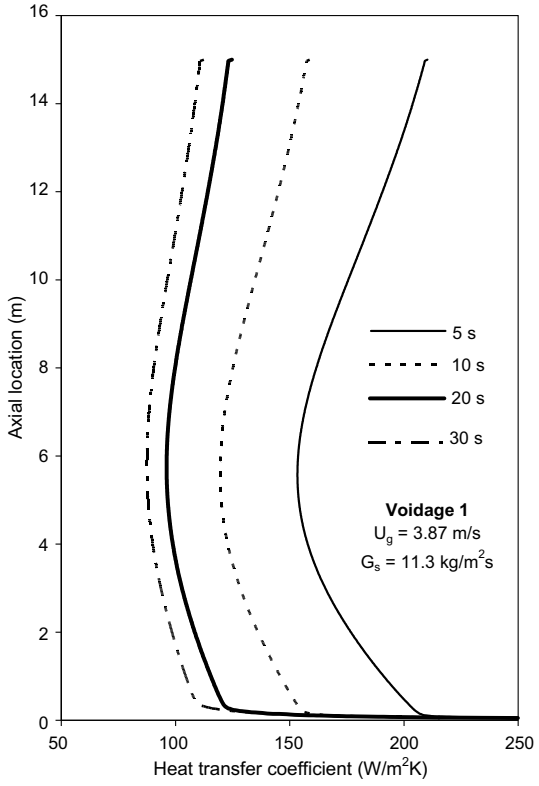

Fig. 4. Variation in axial bed-to-wall heat transfer coefficient with time for one particular case of average voidage distribution: *Voidage 1* in Fig. 2.

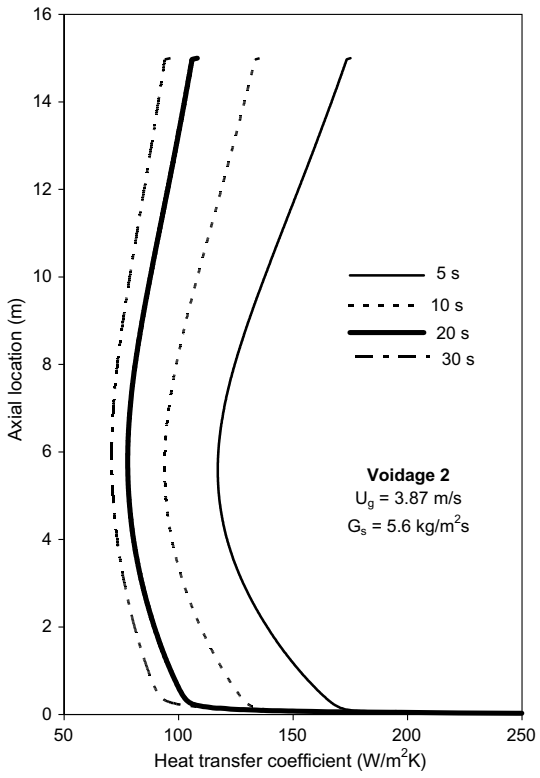

Fig. 5. Variation in axial bed-to-wall heat transfer coefficient with time for one particular case of average voidage distribution: *Voidage 2* in Fig. 2.

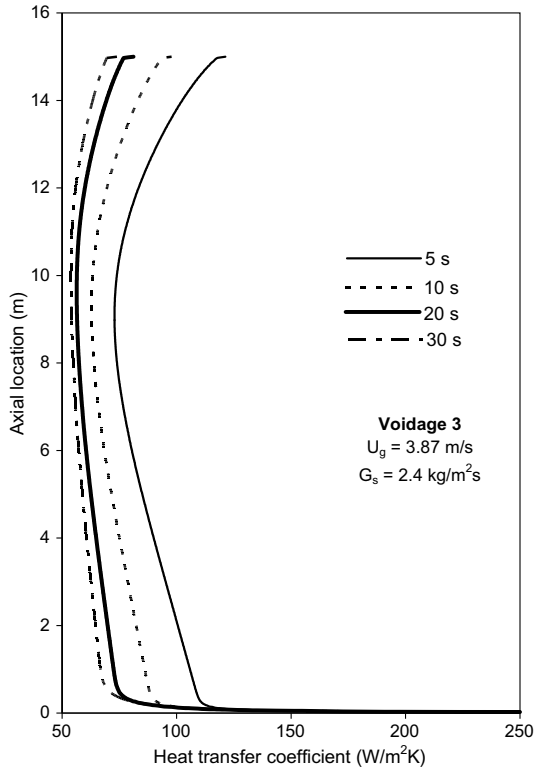

Fig. 6. Change in axial bed-to-wall heat transfer coefficient with time for one particular case of average voidage distribution: *Voidage 3* in Fig. 2.

to 2 and 3, due to lesser particles in that zone (Fig. 2). These three cases show the impact of average bed voidage on the near wall axial heat transfer process.

5.2. Effect of horizontal voidage distribution

The horizontal voidage distribution as estimated from Eq. (1) by Issangya et al. [13] at a location in the top region of the riser column for the three voidage cases is shown in Fig. 7. The influence of average voidage on the horizontal voidage is evident; the higher voidage case of 3 has the most voidage across the riser diameter while the voidage 1 has lower voidage throughout. This change in the voidage across the diameter as well as along the height will impact the heat transfer significantly. The effect of horizontal change in voidage information on heat transfer is observed by comparing a case when using the mass flux balance model of He et al. [4], for the given axial voidage profile at the same hydrodynamic conditions (of the Voidage 2 profile), the corresponding axial core and annulus voidage (no change in horizontal voidage) along with the heat transfer values are estimated. The comparison is shown in Fig. 8 where the profile of the average voidage is well reflected in the variable 'horizontal voidage' case whereas not much variation along the height is observed for the 'fixed voidage' case. The heat transfer values for 'horizontal voidage' are lower and has more realistic trend (based on general range of experimental heat transfer coefficients reported in literature, Basu and Nag [19], Ma and Zhu [20]) when compared to the 'fixed horizontal voidage' case at both the times as shown in Fig. 8.

5.3. Effect of bed initial temperature

The change in axial bed-to-wall heat transfer coefficient for three different bed initial temperatures are compared in Fig. 9: T_b (1100 K), T_{avg} (850 K) and Linear (the initial bed temperature is allowed to change linearly from top to bottom from 900 to 1100 K, respectively). The first two are constant initial temperatures at all the nodes while the third (Linear) has different initial temperature at each axial location (fixed for all horizontal nodes in that axial location). The fixed temperature conditions show similar trends with lower heat transfer value for the T_{avg} case. The linearly changing bed initial temperature has different profile in the upper regions of the bed. The real CFB unit is bound to have a temperature gradient from bottom to top with a range of difference from 100 to 200 K. Thus, the effect of the voidage profile in the top regions may not affect the heat transfer coefficient when the bed temperature at the top is lower than at the bottom region of the riser.

5.4. Effect of axial bed temperature

The heat transfer coefficient estimations discussed in Sections 4.1 and 4.3 (denoted in the plot as 'h-Tbpg') are compared for two different bed initial temperatures in Fig. 10. There is no difference when the bed initial temperature is at T_b, thus supporting the

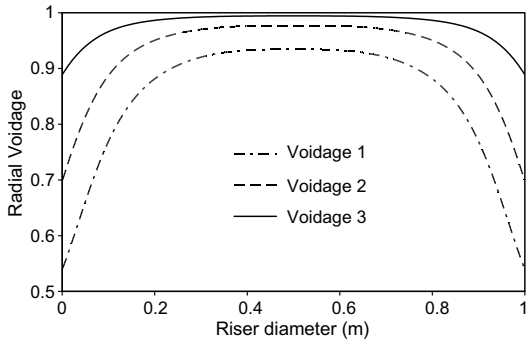

Fig. 7. Variation in horizontal voidage distribution corresponding to the three average axial voidage in Fig. 2 at one particular axial location of the riser.

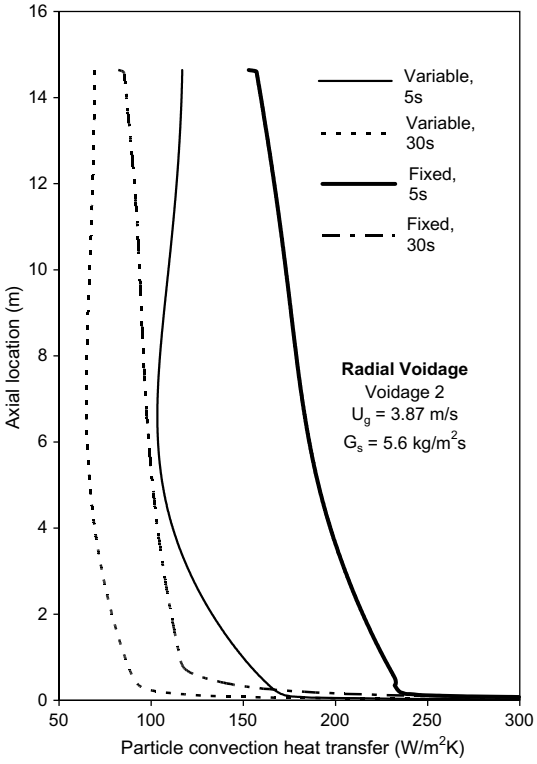

Fig. 8. Variation in axial bed-to-wall heat transfer coefficient for variable and fixed horizontal voidage distribution at two different times.

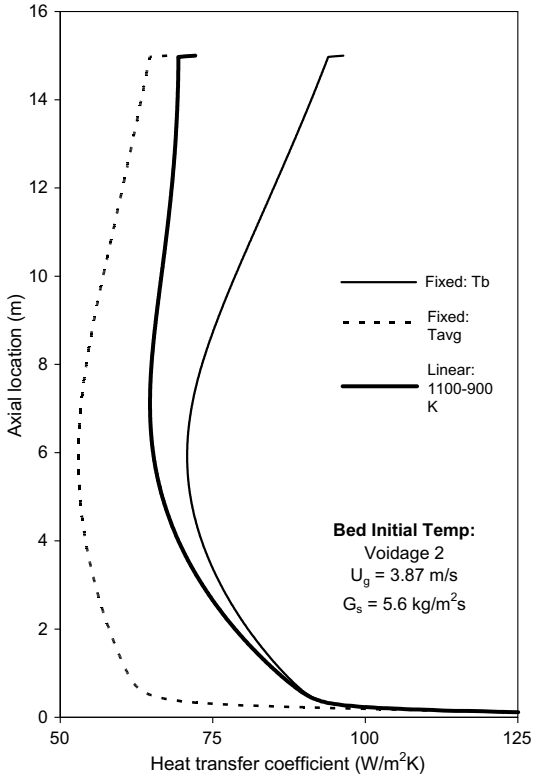

Fig. 9. Variation in axial bed-to-wall heat transfer coefficient for three different bed initial temperatures: (i) fixed higher temperature (T_b) for the entire bed, (ii) fixed average temperature (T_{avg}) for the entire bed and (iii) linearly varying temperature along the height.

heat transfer estimation in Section 4.1 as well as Section 4.3 (using the horizontal voidage and temperatures of particle and gas

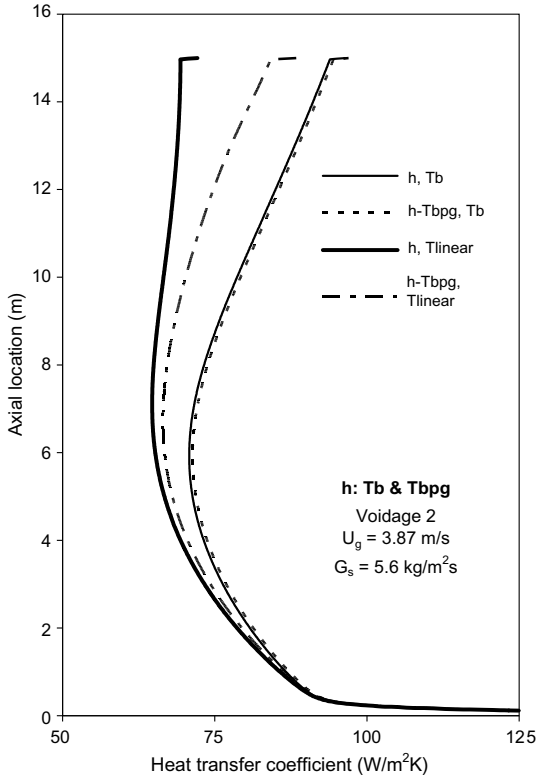

Fig. 10. Variation in axial bed-to-wall heat transfer coefficient for two different heat transfer coefficient estimations as discussed in Section 4.

nodes). There is significant difference in heat transfer values for a linear change in initial bed temperature especially in the top region. Here the axial bed temperature makes the difference due to the horizontal voidage distribution along the height. This brings back effect of solids concentration into the linear bed temperature change as would show up in real CFB units.

5.5. Effect of gas gap

It is generally agreed [19] that a gas gap exists between the particles and the wall in the annulus region. The presence of thin gas gap/layer between the wall and the cluster throughout its fall was reported by Lints and Glicksman [21] with a correlated thickness of $d_p 0.0282(1-\bar{\varepsilon})^{-0.590}$. If a similar gas gap is applied for the current 2D grid for a single node next to the wall along the height (having a maximum thickness of about 1 mm), the corresponding change in heat transfer value for two different bed initial temperatures is shown in Fig. 11. With the presence of the gas gap there is significant reduction (up to 25%) in heat transfer to the wall especially under higher initial bed temperatures. The addition of gas gap should be considered when comparing with experimental data for axial heat transfer profiles.

5.6. Annulus-to-wall heat transfer coefficient

Even though there is no annulus and core segregation in the grid properties, it is achieved by using the annulus thickness correlation from Harris et al. [22] as given here which varies axial for a given location within the riser column,

$$\delta_a = 0.5D\left[0.4014\mathrm{Re}_D^{0.0585}\bar{\varepsilon}^{(-0.0247)}\left(\frac{H-dy^*j}{H}\right)^{-0.0663}\right] \quad (23)$$

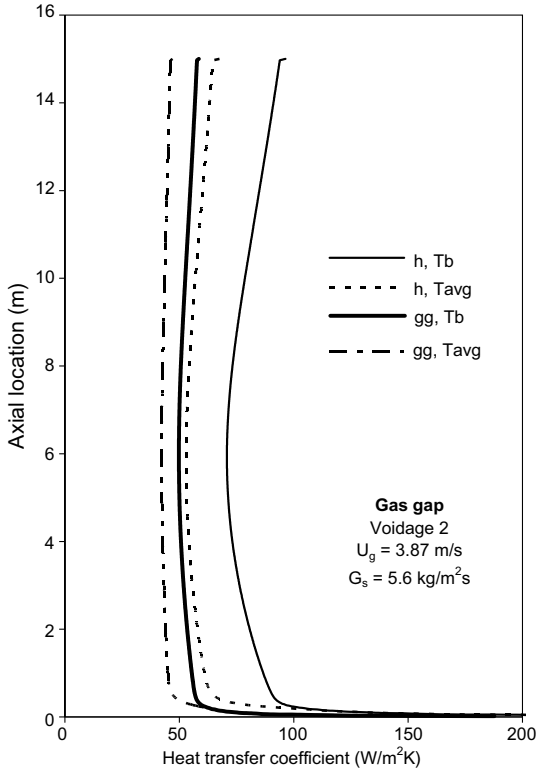

Fig. 11. Variation in axial bed-to-wall heat transfer coefficient compared between, with and without the presence of gas gap between the wall and the gas–solid suspension near the wall.

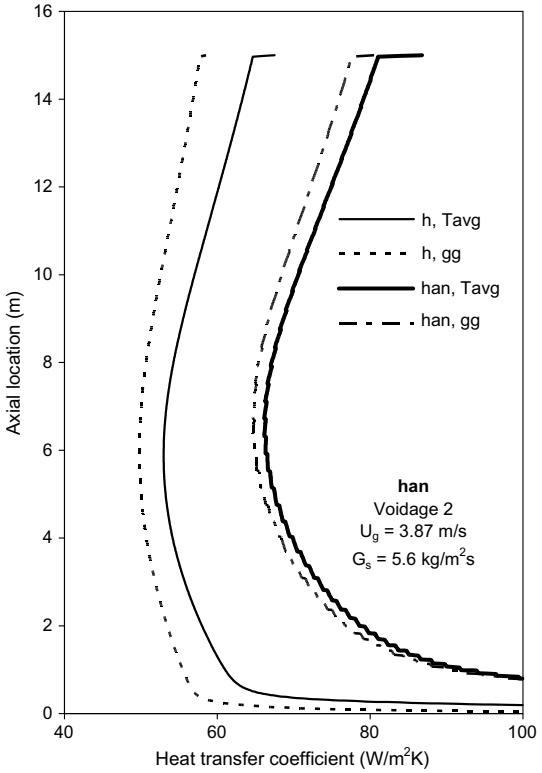

Fig. 12. Variation in axial bed-to-wall heat transfer coefficient compared with axial annulus-to-wall heat transfer coefficient estimation.

This expression considers the effect of gas velocity, solids circulation rate and exit shape apart from the riser dimensions. Single annulus and core temperature is obtained by averaging all the temperature nodes within that thickness to get the average annulus and core temperatures. This is used to estimate the annulus-to-wall heat transfer coefficient as discussed in Section 4.2. The difference in the bed-to-wall and annulus-to-wall heat transfer coefficients for average bed initial temperatures and with gas gap is shown in Fig. 12. The annulus-to-wall values are higher for both initial temperature and the gas gap cases compared to the bed-to-wall estimation. The gas gap case has T_b as the initial bed temperature, but still its value is lower than the average initial temperature case. This is because the bulk annulus temperature reduces significantly due to the presence of gas gap, which apart from being a resistance to the heat transfer will also reduce the local temperature of the annulus region near the wall.

5.7. Validation with experimental trends in published literature

The time variation of axial heat transfer by fixing the bed hydrodynamics is very difficult to measure and those available in the literature are average values. Since the axial heat transfer process happens repeatedly with combinations of different voidage profiles (due to changes in local hydrodynamics), a sustainable axial bed temperature is established eventually when the operating conditions remain the same. The steady state heat transfer values measured and reported from an experimental setup should be observed as average of quasi-steady state conditions, because the local hydrodynamics is not constant with time in these experiments (which is the fundamental characteristic of CFB combustors), thus making it difficult to be compared with the results from the current work. Some of the steady state experimental data available for axial heat transfer profile in the literature include Ma and Zhu [1,20], He et al. [4], Hua et al. [3] and Koksal et al. [5]. There is one more difficulty in comparing model values one-on-one with experimental data from these literatures; the size of the column used in these experiments is smaller than that used in the current model. The hydrodynamic parameters in Eqs. (1) and (23) have limitations for lower diameters (anything less than 0.5 m makes the model unstable) and the heat transfer values in the literature are measured for smaller diameters meaning higher heat transfer values as reported in these literatures. That is the reason for comparing just the trends rather than the values. The current model trends are compared with Ma and Zhu [20] profiles and shows similar heat transfer trends with close agreement (60–70%) under similar range of operating conditions (G_s and U_g). As it can be observed from Ma and Zhu [20] – (Fig. 3(a), pp. 984) – the operating conditions used in this experimental data is quite different from that used in the current work and the diameter of the column used is 100 mm while in the current work it is 1 m. Though similar trends of the heat transfer values (i.e., higher at the bottom, reduces in the middle and increases at the top) are observed in the current work. The measurement of resistance to heat transfer due to the presence of gas gap alone is also difficult and thus is not found in the literature to make a comprehensive comparison but the average value between with and without gas gap is appropriate to compare with averaged steady state experimental data.

6. Conclusions

In the current work, the axial bed-to-wall heat transfer coefficients for the CFB combustor are estimated using the gas–solid thermal energy balance model for three different averaged axial voidage profiles (form published experimental data). The analyses and results provide the following inferences:

- *Effect of axial voidage distribution:* Axial heat transfer varies along the height from bottom to top (both higher than in the middle) of the riser column. The change in axial heat transfer with time for the three axial voidage distributions when observed together shows the range of heat transfer values the combustor will undergo when the mass flux changes with time.
- *Effect of horizontal voidage distribution:* The difference in heat transfer values for fixed and variable horizontal voidage distributions is significant showing the importance of considering horizontal voidage variation while estimating the axial heat transfer coefficients.
- *Effect of bed initial temperature:* The analysis with three different bed initial temperature conditions shows that the axial heat transfer profile depends not only on the voidage distribution but also on the local temperature gradients.
- *Annulus-to-wall heat transfer:* The heat transfer estimation based on three different temperature conditions (bed-to-wall, annulus-to-wall and axial bed temperature) shows significant variations suggesting that the use local temperature differences instead of bed temperature.
- *Effect of gas gap:* The presence of even a thin layer of gas gap (without particles) between the wall and the gas–solid phase near the wall reduces the axial heat transfer considerably (up to 25% for a maximum thickness of 1 mm).
- *Time analysis:* Fixing the hydrodynamics with time and observing the instantaneous heat transfer behaviour along the height of the riser column shows that, only limited time (less than 10 s) is available for the wall to transfer heat from high temperature gas–solid suspension thus reducing the average heat coefficient.

This work proves the importance of proper voidage estimation by fixing it with time and in a different analysis changing it horizontally at every axial location to show the sensitivity in heat transfer estimation (which is not easy to measure). Significant information is conveyed in the current work through the axial heat transfer trends (proportional behaviour due to parametric change), that is, the variation of axial heat transfer with respect to changes in time, axial and horizontal voidage, temperature conditions and gas gap.

Acknowledgements

The authors kindly acknowledge the financial support for the present project from NSERC, Canada through Discovery Grant Program. The work was done at Department of Mechanical Engineering, University of New Brunswick, Fredericton, NB, Canada.

References

[1] Y. Ma, J.X. Zhu, Heat transfer between gas–solids suspension and immersed surface in an up flow fluidized bed (riser), Chem. Eng. Sci. 55 (2000) 981–989.
[2] E.R. Monazam, L.J. Shadle, J.S. Mei, J. Spenik, Identification and characteristics of different flow regimes in a circulating fluidized bed, Powder Technol. 155 (2005) 17–25.
[3] Y. Hua, G. Flamant, J. Lu, D. Gauthier, 3D modeling of radiative heat transfer in circulating fluidized bed combustors: influence of the particulate composition, Int. J. Heat Mass Transfer 48 (2005) 1145–1154.
[4] Q. He, F. Winter, J.D. Lu, Analysis of the heat transfer mechanism in high-temperature circulating fluidized beds by a numerical model, Trans. ASME 124 (2002) 34–39.
[5] M. Koksal, M.R. Golriz, F. Humdullahpur, Thermal aspects of a circulating fluidized bed with air staging, Int. J. Energy Res. 29 (2005) 923–935.
[6] B.V. Reddy, P.K. Nag, Axial and radial heat transfer studies in a circulating fluidized bed, Int. J. Energy Res. 21 (1997) 1109–1122.
[7] D. Xie, B.D. Bowen, J.R. Grace, C.J. Lim, Two-dimensional model of heat transfer in circulating fluidized beds. Part I: Model development and validation, Int. J. Heat Mass Transfer 46 (2003) 2179–2191.
[8] D. Xie, B.D. Bowen, J.R. Grace, C.J. Lim, Two-dimensional model of heat transfer in circulating fluidized beds. Part II: Heat transfer in a high density CFB and sensitivity analysis, Int. J. Heat Mass Transfer 46 (2003) 2193–2205.
[9] E. Helland, R. Occelli, L. Tadrist, Numerical study of cluster formation in a gas-particle circulating fluidized bed, Powder Technol. 110 (2000) 210–221.
[10] J.C. Moran, L.R. Glicksman, Experimental and numerical studies on the gas flow surrounding a single cluster applied to a circulating fluidized bed, Chem. Eng. Sci. 58 (2003) 1879–1886.
[11] L. Huilin, S. Qiaoqun, H. Yurong, S. Yongli, J. Ding, L. Xiang, Numerical study of particle cluster flow in risers with cluster-based approach, Chem. Eng. Sci. 60 (2005) 6757–6767.
[12] N.V. Gnanapragasam, B.V. Reddy, Numerical modeling of bed-to-wall heat transfer in a circulating fluidized bed combustor based on cluster energy balance, Int. J. Heat Mass Transfer 51 (2008) 5260–5268.
[13] A.S. Issangya, J.R. Grace, D. Bai, J. Zhu, Radial voidage variation in CFB risers, Can. J. Chem. Eng. 79 (2001) 279–286.
[14] J.F. Richardson, P. Ayers, Heat transfer between particles and gas in a fluidized bed, Trans. Inst. Chem. Eng. 37 (1959) 314–322.
[15] N.V. Gnanapragasam, Heat transfer investigations in a circulating fluidized bed combustor, PhD Thesis, University of New Brunswick, Fredericton, Canada, 2007.
[16] M. Eriksson, M.R. Golriz, Radiation heat transfer in circulating fluidized bed combustors, Int. J. Thermal Sci. 44 (2005) 399–409.
[17] S. Patankar, Numerical Heat Transfer and Fluid Flow, Hemisphere Publication Cooperation, New York, 1980.
[18] H.K. Versteeg, W. Malalasekera, An Introduction to Computational Fluid Dynamics, Prentice Hall, New York, 1995.
[19] P. Basu, P.K. Nag, Heat transfer to walls of a circulating fluidized bed furnace, Chem. Eng. Sci. 51 (1996) 1–26.
[20] Y.L. Ma, J.X. Zhu, Heat transfer in the downer and the riser of a circulating fluidized bed – a comparative study, Chem. Eng. Technol. 24 (2001) 85–90.
[21] M.C. Lints, L.R. Glicksman, Parameters governing particle to wall heat transfer in a circulating fluidized bed, in: A.A. Avidan (Ed.), Circulating Fluidized Bed Technology IV, AIChE, New York, 1994, pp. 63–82.
[22] A.T. Harris, R.B. Thorpe, J.F. Davidson, Characterisation of the annular film thickness in circulating fluidized-bed risers, Chem. Eng. Sci. 57 (2002) 2579–2587.
[23] G. Flamant, Tranfert de chaleur couples dans les lits fluidises a haut temperature, Application a la conversion thermique de l'energie solaire, these de docteur Ea-Science, 93, 1985.